


Cite this: *J. Mater. Chem. A*, 2017, 5, 18457Received 5th July 2017
Accepted 15th August 2017

DOI: 10.1039/c7ta05832b

rsc.li/materials-a

Li-ion transport in a representative ceramic–polymer–plasticizer composite electrolyte: $\text{Li}_7\text{La}_3\text{Zr}_2\text{O}_{12}$ –polyethylene oxide–tetraethylene glycol dimethyl ether†

Jin Zheng,^a Heather Dang,^a Xuyong Feng,^a Po-Hsiu Chien^a and Yan-Yan Hu^{†*}

Ceramic–polymer hybrids carry the promise of forming composite electrolytes with high ionic conductivity, good stability and compatibility with electrodes, and excellent mechanical properties that cannot be achieved with conventional ceramic or polymer ion conductors. Small molecule additives often further enhance ion conduction. This work employs a representative composite comprising a ceramic Li-ion conductor, garnet-type $\text{Li}_7\text{La}_3\text{Zr}_2\text{O}_{12}$ (LLZO), a polymer Li-ion conductor, polyethylene oxide (PEO), and an additive, tetraethylene glycol dimethyl ether (TEGDME). All the Li sites in bulk LLZO, PEO, and TEGDME, and at the interfaces of PEO/LLZO, PEO/TEGDME, and LLZO/TEGDME, have been clearly identified with high-resolution Li NMR. It is determined using the $^6\text{Li} \rightarrow ^7\text{Li}$ isotope replacement strategy that Li-ion transport in this composite occurs mainly via TEGDME-associated phases. Changes in the bulk and interfacial structures of the composite will likely alter Li-ion pathways and thus lead to variation in ionic conductivity. As an example, the composite structure evolves over time, which results in a decrease in active Li sites and degradation of ionic conductivity.

Introduction

Li-ion batteries (LIBs) are crucial components in a wide range of technologies, from portable electronic devices and electric vehicles to large-scale energy storage systems.^{1,2} Since LIBs were first commercialized in 1991 by Sony in Japan, developing suitable electrolytes for LIBs with high energy density, long lifespan, and high safety has been a long-term challenge.^{3,4} In conventional LIBs, liquid electrolytes are widely used, which are Li salts dissolved in organic solvents. However, because of their inadequate chemical stability, liquid electrolytes cause severe safety issues, notably corrosion and flammability.⁵ Another associated problem is Li dendrite formation during

charge–discharge cycling, which results in internal short circuits and becomes the flash point of explosion.^{6,7}

A promising strategy to solve these problems is to replace liquid electrolytes with nonflammable solid electrolytes (SEs). Currently, there are three classes of SEs: inorganics (ceramics and glasses), polymers, and composite electrolytes.^{8,9} Inorganic electrolytes exhibit high ionic conductivity (10^{-2} – 10^{-4} S cm^{-1} at room temperature),^{10–12} but they are rigid and brittle, resulting in poor contact with electrodes and mechanical failure.^{13–15} Polymer electrolytes are flexible, but their low conductivity ($<10^{-6}$ S cm^{-1}) at ambient temperature and poor stability at high temperatures limit their utilization in LIBs.^{16,17} Composite electrolytes combine the advantages of both organics and inorganics, carrying the promise of forming systems with high ionic conductivity, good stability, and favorable mechanical properties.^{18–21}

Despite the fact that composite electrolytes may provide a solution to the inherent problems associated with inorganic or organic solid electrolytes, finding the best combination and engineering them to obtain optimal properties are not trivial. Inorganic electrolytes require compact packing to deliver high ionic conductivity, and incorporating polymers into them often reduces the packing density, disrupts the conduction network, and limits the material processing temperature. Integrating a small amount of inorganic fillers into polymer electrolytes has been proven to significantly improve their conductivity and stability.^{20,22–24} Small molecular additives are often employed to further enhance the ionic conductivities of SEs. For instance, adding plasticizers is one of the most common approaches, which can decrease the crystallinity of polymers and thus increase the mobility of Li ions in the electrolytes. Plasticizers, such as tetraethylene glycol dimethyl ether (TEGDME), ethylene carbonate (EC) and succinonitrile (SN), have successfully increased the ionic conductivity of polymer and composite electrolytes by orders of magnitude.^{25–28}

The synergistic combination of ion conducting polymers and inorganics with additives leads to a highly promising solution for fulfilling all the requirements for the next generation of solid

^aDepartment of Chemistry and Biochemistry, Florida State University, Tallahassee, FL 32306, USA. E-mail: hu@chem.fsu.edu

^bCenter of Interdisciplinary Magnetic Resonance, National High Magnetic Field Laboratory, 1800 East Paul Dirac Drive, Tallahassee, FL 32310, USA

† Electronic supplementary information (ESI) available. See DOI: 10.1039/c7ta05832b

electrolytes. However, current composite systems are far from ideal. Developing effective strategies for further performance enhancement necessitates a fundamental understanding of how the composites work to achieve high conductivity and stability and good mechanical properties. It is particularly critical to elucidate what roles each component plays in ion conduction.

In this contribution, we choose a representative system of composite electrolytes, LLZO-PEO (LiClO_4)-TEGDME, to illustrate the part that each component plays to form the Li-ion transport pathways. In addition, the stability of the composite electrolyte is also examined. The approach employed in this study is high-resolution solid-state nuclear magnetic resonance (NMR) combined with ${}^6\text{Li} \rightarrow {}^7\text{Li}$ isotope replacement.^{29,30} High-resolution ${}^6\text{Li}$ NMR identifies all the local environments in LLZO, PEO, TEGDME and interfaces where Li ions reside and Li-ion dynamics within these local structures. Isotope replacement NMR maps the Li-ion movement through these local environments to form a transport pathway. Stability studies have shed light on the evolution of structure and composition over time, and the associated performance degradation of the composite electrolyte. The results provide insights into the functional components in the complex composite electrolytes for fast ion-conduction. The new knowledge obtained here will be useful for materials design, synthesis, and engineering to obtain high performance electrolytes used in energy storage technologies.

Experimental methods

Synthesis of cubic-LLZO

Al-doped cubic-LLZO was synthesized using the sol-gel method. The starting materials, LiOH (Sigma Aldrich, 98%), $\text{La}(\text{NO}_3)_3 \cdot 6\text{H}_2\text{O}$ (Alfa Aesar, 99.9%), $\text{Zr}(\text{OC}_4\text{H}_9)_4$ (Sigma Aldrich, 80 wt% in 1-butanol), $\text{Al}(\text{NO}_3)_3 \cdot 9\text{H}_2\text{O}$ (Alfa Aesar, 98%), and citric acid (Sigma Aldrich, 99%), were dissolved in dilute HNO_3 . The molar ratio of Li : La : Zr : Al : citric acid in the solution was 8.4 : 3.0 : 2.0 : 0.2 : 5.0. 20 wt% excess LiOH was added to compensate for the loss of Li during the heating process. Citric acid was used as a complexing agent. The solution was stirred and heated at 80 °C overnight to gradually remove water and then dried at 200 °C for 2 h. A solid, white foam was obtained and crushed into powders, which were calcined at 290 °C for 2 h. The black powders were then sintered at 900 °C for 8 h.

Preparation of composite films

The 40 wt% LLZO-40 wt% PEO (LiClO_4)-20 wt% TEGDME composite electrolyte was prepared by a solution casting method. Polyethylene oxide (PEO) (Sigma Aldrich, M_w : 400 000), LiClO_4 (Sigma Aldrich, 98%), and tetraethylene glycol dimethyl ether (TEGDME) (Sigma Aldrich, 99%) were carefully dried and dissolved in anhydrous acetonitrile at an [EO] : [Li] ratio of 18 : 1. The solution was stirred in an argon-filled glovebox for 24 h and mixed with the as-prepared cubic-LLZO. The mixture was ball-milled for 2 h to obtain a homogenous slurry and cast on a flat Teflon plate using a doctor blade. To evaporate the

solvent, the slurry was dried in the glovebox for 12 h. The thickness of the obtained composite film ranged from 50 to 70 μm .

Electrochemical tests

The composite film was stored inside an argon-filled glovebox, without contact with Li metal. Samples were extracted from the same film 0, 2, 5, 10, and 20 days after it was made. The extracted samples were then assembled with Li metal for impedance tests. The contact time of the electrolyte with Li metal was about the duration of the impedance measurements. Therefore, the Li/electrolyte interfacial conditions were expected to be the same for all the measurements, which was confirmed by the very similar interfacial resistance values (Table S4†). The AC impedance measurements were performed on a Gamry Reference 600+ with an AC amplitude of 100 mV in the frequency range of 5 MHz to 1 Hz. The ionic conductivity of the composite electrolytes was calculated using the following equation: $\sigma = L/(R_b \times A)$, where L is the thickness of the composite film, R_b is the bulk resistance and A is the contact area between the electrolyte and the electrode.

Isotope exchange

${}^7\text{Li} \rightarrow {}^6\text{Li}$ isotope exchange for determining the Li-ion transport pathways was performed as described in the following: a biased potential was applied to a symmetric cell made with ${}^6\text{Li}$ -enriched Li metal foil as the electrodes, ${}^6\text{Li}|\text{LLZO-PEO}(\text{LiClO}_4)\text{-TEGDME}|{}^6\text{Li}$, to drive ${}^6\text{Li}$ ions from one ${}^6\text{Li}$ electrode to exchange with ${}^7\text{Li}$ in the composite electrolyte before reaching the other ${}^6\text{Li}$ electrode. The direction of the applied potential was switched at 5 min intervals. A constant current density of 7.2 $\mu\text{A cm}^{-2}$ was used. The test was carried out on a LANHE (CT2001A) battery testing system.

NMR characterization

Solid-state ${}^6\text{Li}$ and ${}^7\text{Li}$ NMR experiments were carried out on a Bruker Avance III-500 spectrometer operating at ${}^6\text{Li}$ and ${}^7\text{Li}$ Larmor frequencies of 73.6 and 194.4 MHz. ${}^6,7\text{Li}$ Magic-Angle Spinning (MAS) measurements were performed with a 2.5 mm Bruker HXY probe and the samples were spun at 25 kHz for direct polarization and 10 kHz for ${}^1\text{H}$ - ${}^6,7\text{Li}$ cross polarization. The lengths of 90° NMR radio frequency pulses were 4.75 μs for ${}^6\text{Li}$, 2.00 μs for ${}^7\text{Li}$, and 2.55 μs for ${}^1\text{H}$. The recycle delays were 50 s for ${}^6,7\text{Li}$. LiCl (s) with a ${}^6,7\text{Li}$ resonance at 0 ppm was used as the chemical shift reference.

Results and discussion

Fig. 1a schematically shows the preparation process of the composite electrolyte, LLZO-PEO (LiClO_4)-TEGDME. The detailed procedure is described in the Experimental section. The obtained composite electrolyte is a flexible film with a thickness of 50–70 μm , containing 40 wt% LLZO, 40 wt% PEO and 20 wt% TEGDME. The composite electrolyte, LLZO-PEO (LiClO_4)-TEGDME, is depicted as LLZO particles distributed within the PEO polymer matrix. The LLZO-PEO interface is

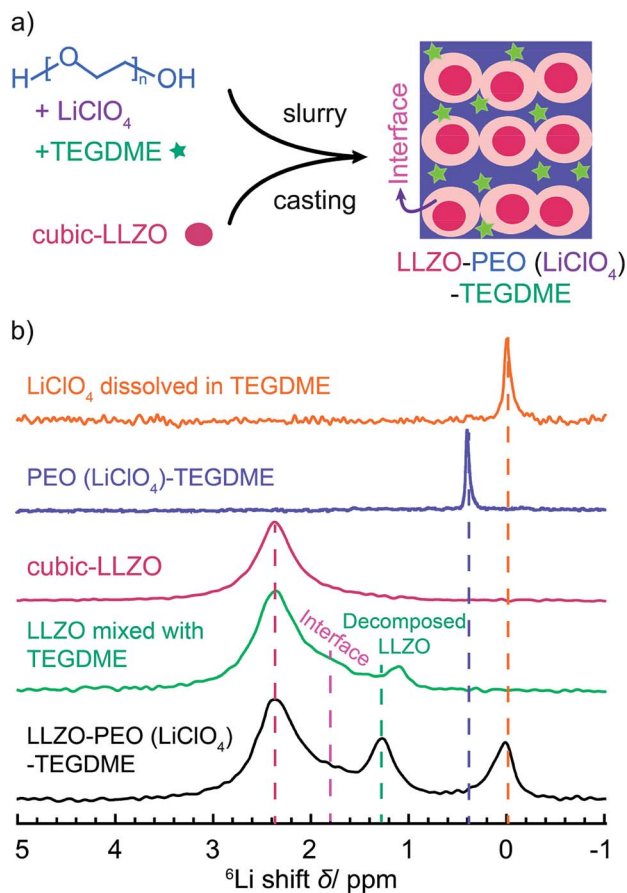


Fig. 1 (a) Preparation of the LLZO-PEO (LiClO_4)-TEGDME composite film; (b) ^6Li MAS NMR spectra of (from top to bottom) LiClO_4 dissolved in TEGDME, PEO (LiClO_4)-TEGDME, pure cubic LLZO, LLZO mixed with TEGDME, and LLZO-PEO (LiClO_4)-TEGDME.

also shown. The TEGDME additive is distributed within the LLZO-PEO composite. To understand the structure of the complex composite LLZO-PEO (LiClO_4)-TEGDME, high-resolution solid-state ^6Li MAS NMR was employed to examine all constituents individually and their combinations, as shown in Fig. 1b. The ^6Li NMR spectrum of LiClO_4 dissolved in TEGDME shows a resonance at 0 ppm. LiClO_4 in the PEO-TEGDME matrix exhibits a relatively sharp peak at 0.4 ppm. The ^6Li NMR signal of pure cubic-LLZO is seen at 2.4 ppm. When LLZO is mixed with TEGDME, in addition to the 2.4 ppm resonance, two new peaks at 1.2 and 1.8 ppm appear and are assigned to Li at the LLZO-TEGDME interface and decomposed LLZO dissolved in TEGDME. When LLZO particles are dispersed in TEGDME, the colour of the mixture turns from transparent to yellowish, suggesting decomposition of LLZO in TEGDME. The assignment of decomposed LLZO is further supported by a series of ball-milling experiments (Fig. S1[†]). The 1.2 ppm resonance grows more intense when the ball-milling speed and duration increase during the LLZO-PEO (LiClO_4) composite preparation. This decomposed LLZO phase shows a much longer ^7Li T_1 relaxation time (~ 11.3 s) compared with LLZO (~ 1.1 s) (Fig. S2 and Table S1[†]), suggesting that they are not spatially close; otherwise spin exchange would occur to homogenize the T_1

relaxation times. It is worth mentioning that the decomposed LLZO plays an important role in Li-ion transport, which will be discussed later. The interfacial Li resonance at 1.8 ppm will be further validated using data presented in Fig. 2. In the ^6Li NMR spectrum of LLZO-PEO (LiClO_4)-TEGDME, the signal from LiClO_4 in TEGDME is still around 0 ppm, but becomes much broader compared with that of LiClO_4 in pure TEGDME. The large breadth of the resonance results from a broad distribution of solvated environments. The LLZO absorbs a fraction of added TEGDME, reducing the ratio of TEGDME to PEO. It is known that TEGDME has been used as an important plasticizer in PEO polymer electrolytes to prevent PEO crystallization. The mobility of TEGDME within the PEO matrix will be slower than that of

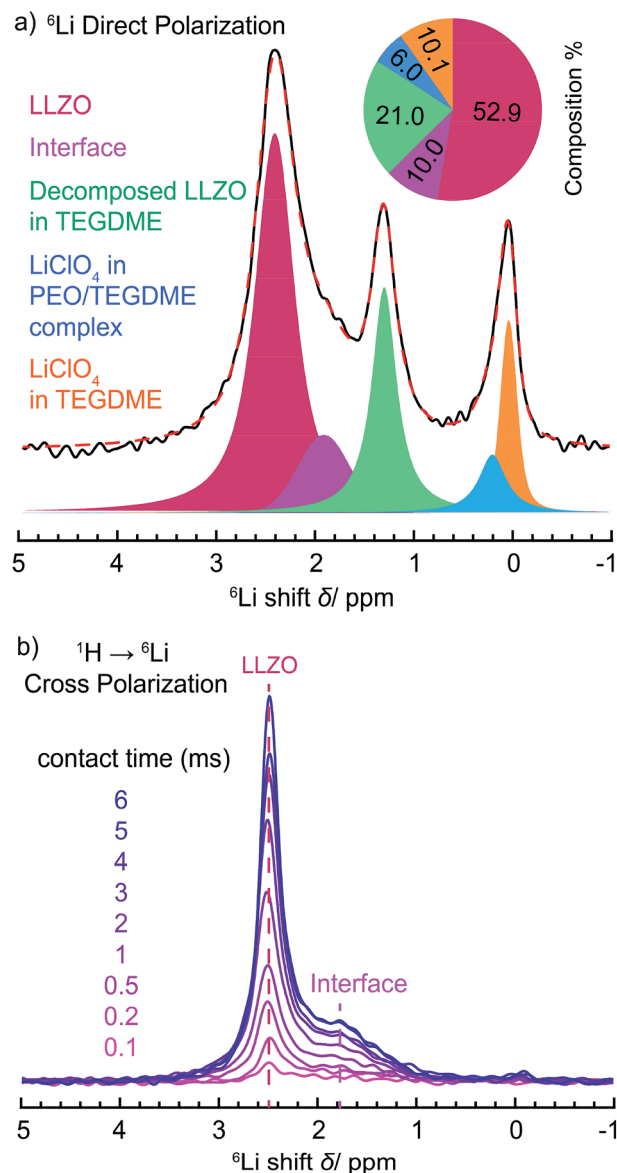


Fig. 2 (a) ^6Li direct polarization (DP) NMR spectrum, simulation, assignments and quantification results of the LLZO-PEO (LiClO_4)-TEGDME composite; (b) ^1H - ^6Li cross polarization (CP) NMR spectra of the LLZO-PEO (LiClO_4)-TEGDME composite with various CP contact times.

pure TEGDME; thus the motional averaging of the anisotropy from various solvated Li environments is less efficient than that in pure TEGDME, leading to a broader resonance in ${}^6\text{Li}$ NMR. The LLZO and PEO/LLZO interface resonances remain approximately the same as those in LLZO–TEGDME. The resonance from decomposed LLZO in TEGDME shifts slightly to a lower field with a larger ppm value, likely due to the participation of the PEO matrix. The increased intensity suggests more LLZO decomposition, possibly from the mixing process by ball-milling.

Fig. 2a presents simulations, assignments, and quantification results of ${}^6\text{Li}$ direct polarization (DP) NMR for LLZO–PEO (LiClO_4)–TEGDME. Detailed analysis of the spectrum shows 5 distinct components: cubic-LLZO at 2.4 ppm, the PEO/LLZO interface at 1.8 ppm, decomposed LLZO in TEGDME at 1.2 ppm, LiClO_4 in the PEO/TEGDME complex at 0.2 ppm, and LiClO_4 in TEGDME at 0.0 ppm. Quantification based on the area integrals of the simulated NMR resonances shows 52.9 mol% Li from LLZO, 10.0 mol% Li at the PEO/LLZO interface, 21.0 mol% Li from LLZO in TEGDME, 6.0 mol% Li from LiClO_4 in the PEO/TEGDME complex, and 10.1 mol% Li from LiClO_4 in TEGDME. To further probe interfacial Li ions in LLZO–PEO (LiClO_4)–TEGDME, ${}^1\text{H}$ – ${}^6\text{Li}$ cross polarization (CP) NMR spectra were collected using various CP contact times (Fig. 2b). The abundant ${}^1\text{H}$ spins in the organic phases (PEO and TEGDME) were polarized first, and then the magnetization was transferred from ${}^1\text{H}$ to less abundant ${}^6\text{Li}$ spins in LiClO_4 and LLZO, and at interfaces *via* heteronuclear dipolar interaction between ${}^1\text{H}$ and ${}^6\text{Li}$ spins. The ${}^1\text{H}$ – ${}^6\text{Li}$ dipolar coupling interactions, $D = a\gamma_{\text{H}}\gamma_{\text{Li}}/r^3$, are strongly distance-dependent. With ${}^1\text{H}$ – ${}^6\text{Li}$ CP NMR, Li ions closer to PEO and TEGDME, *e.g.* at the PEO/LLZO interface, can be distinguished from those that are further away, such as those in the LLZO bulk. Longer contact times allow cross-polarization to take place for Li ions further away from ${}^1\text{H}$ spins, resulting in higher intensities of the ${}^6\text{Li}$ NMR signal. ${}^1\text{H}$ – ${}^6\text{Li}$ dipolar coupling interactions can be averaged out by isotropic tumbling motions; therefore, minimal or no dipolar couplings are expected between ${}^1\text{H}$ from fast moving TEGDME molecules and ${}^6\text{Li}$ in Li-containing components. In the ${}^1\text{H}$ – ${}^6\text{Li}$ CP NMR (Fig. 2b), two resonances are observed, one at 2.4 ppm from bulk LLZO and one at 1.8 ppm at the PEO/LLZO interface. The intensity of both components increases with increasing CP contact time. In the CP NMR spectrum with contact time = 6 ms, the interface resonance accounts for 29.0% and LLZO resonance for 71.0%, giving an interface/LLZO ratio of 0.4 : 1. This ratio is significantly higher compared with that in the DP NMR (0.2 : 1), which is because CP NMR driven by ${}^1\text{H}$ – ${}^6\text{Li}$ dipolar couplings preferentially selects the interface spatially closer to the ${}^1\text{H}$ -containing PEO, over LLZO. As is expected, no resonance from Li-species associated with TEGDME is observed, including LiClO_4 and decomposed LLZO in TEGDME. In our previous study on LLZO–PEO (LiClO_4) without additives, the ${}^6\text{Li}$ signal of LiClO_4 in PEO was detected in the ${}^1\text{H}$ – ${}^6\text{Li}$ CP NMR.²⁹ However, in the ${}^1\text{H}$ – ${}^6\text{Li}$ CP NMR spectra of LLZO–PEO (LiClO_4)–TEGDME, the peaks of Li ions in TEGDME or PEO disappeared. This is likely because, in addition to the fast motion of TEGDME molecules, solvated Li ions in TEGDME

also move, thus compromising or eliminating possible ${}^1\text{H}$ – ${}^6\text{Li}$ cross polarization. The absence of LiClO_4 resonance in the ${}^6\text{Li}$ CP NMR spectra (Fig. 2a and b) suggests that all the LiClO_4 salts are associated with TEGDME or in the PEO/TEGDME complex, not in bulk PEO.

To understand the Li-ion conduction mechanism in the complex LLZO–PEO (LiClO_4)–TEGDME composite, a ${}^6\text{Li}$ |LLZO–PEO (LiClO_4)–TEGDME| ${}^6\text{Li}$ symmetric cell was electrochemically cycled using ${}^6\text{Li}$ -enriched metal as electrodes. A constant current of $7.2 \mu\text{A cm}^{-2}$ was applied, the direction of which was changed at 5 min intervals (Fig. 3a). An induced voltage of 75 mV across the symmetric cell was observed. The natural abundance of ${}^7\text{Li}$ is 92.4%, and that of ${}^6\text{Li}$ is 7.6%. During cycling, ${}^6\text{Li}$ ions from one ${}^6\text{Li}$ -enriched electrode moved across the composite electrolyte to reach the other electrode. Along the way, ${}^6\text{Li}$ ions partially replaced ${}^7\text{Li}$ ions in the composite electrolyte. Therefore, the Li ions in the transport pathways will be preferentially ${}^6\text{Li}$ enriched and ${}^7\text{Li}$ deficient. By quantifying the enrichment of ${}^6\text{Li}$ in various Li sites within the composite electrolyte, LLZO–PEO (LiClO_4)–TEGDME, Li-ion pathways can be identified. The ${}^6\text{Li}$ NMR spectra collected for pristine and cycled LLZO–PEO (LiClO_4)–TEGDME composite films are shown in Fig. 3b. Almost no change is observed for bulk LLZO, and only a small increase in the ${}^6\text{Li}$ amount for LLZO at the interface. A significant increase in ${}^6\text{Li}$ is seen for decomposed LLZO dissolved in TEGDME and LiClO_4 in the PEO/TEGDME complex. Correspondingly, a decrease in ${}^7\text{Li}$ resonances was observed for Li in TEGDME (Fig. S3†). The signal for LiClO_4 in TEGDME shifted from 0 ppm to 0.5 ppm, close to the typical Li resonance of Li salts in PEO/TEGDME complex (Fig. 1b). This suggests that the electrochemical cycling facilitates the mixing of PEO and TEGDME in the composite electrolyte. The quantified increase in the ${}^6\text{Li}$ amount of various Li local environments after cycling is shown in Fig. 3c. Among them, a 9.5% increase is observed for LiClO_4 in the PEO/TEGDME complex, 10.1% for decomposed LLZO in TEGDME, and only 1.5% for the PEO/LLZO interface. Table S2† shows the ${}^6\text{Li}$ -enrichment levels of different Li local environments in several aged samples in addition to the freshly prepared LLZO–PEO (LiClO_4)–TEGDME composite, and the results consistently show a significant increase in the ${}^6\text{Li}$ amount for decomposed LLZO and LiClO_4 in TEGDME. Therefore, Li ions prefer to travel through the liquid TEGDME phase within the PEO matrix instead of LLZO or the PEO/LLZO interface. In our previous study on LLZO–PEO (LiClO_4) electrolytes, Li ions were shown to mainly pass through the LLZO network.²⁹ This study suggests that the additive, TEGDME, alters the path of Li ions within the composite electrolyte. This is likely because TEGDME is a good liquid electrolyte, and Li ions are much more mobile in TEGDME than in PEO or LLZO. Thus, Li ions are primarily transported *via* the TEGDME phase.

Higher concentrations of TEGDME often lead to higher ionic conductivities. However, when the ratio of PEO to liquid plasticizer TEGDME is larger than 2 : 1, *i.e.*, the content of TEGDME is >20 wt% in the composites, the composite electrolytes fail to form a solid film, based on our study and other reports.³¹ To investigate the effect of TEGDME at a lower concentration, the

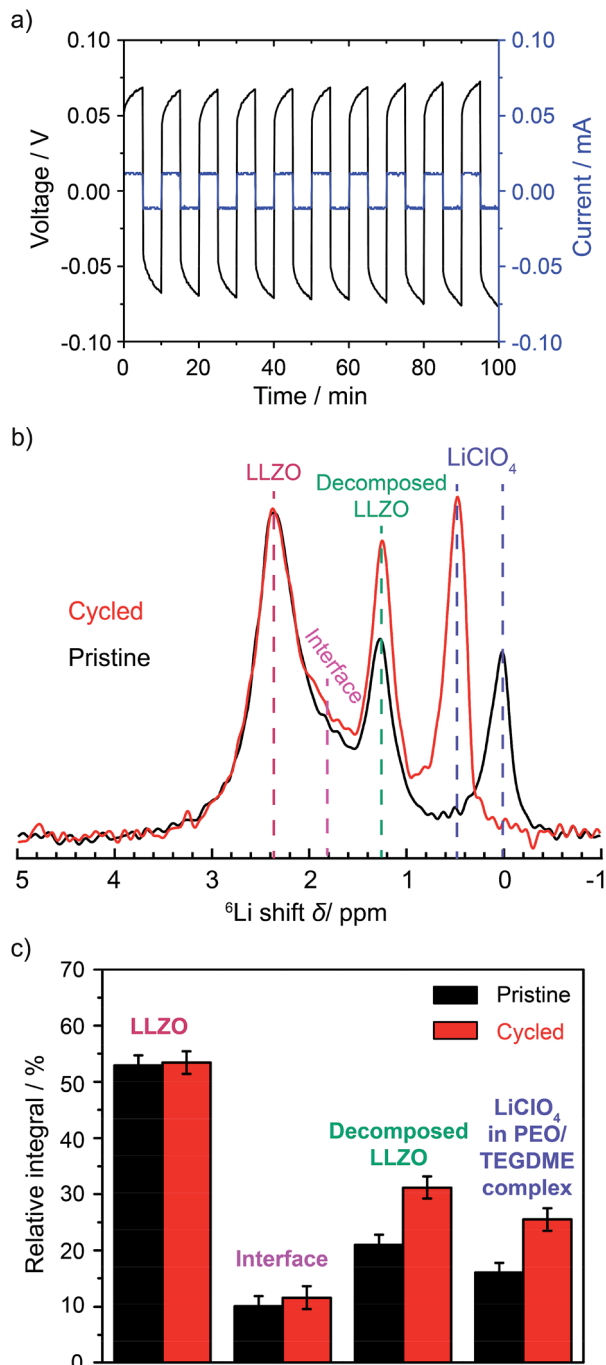


Fig. 3 (a) Voltage profile of the symmetric cell, ${}^6\text{Li}|\text{LLZO-PEO}(\text{LiClO}_4)\text{-TEGDME}|{}^6\text{Li}$, in response to a constant current that changes signs every 5 min; (b) the comparison of the ${}^6\text{Li}$ NMR spectra of the LLZO-PEO (LiClO_4)-TEGDME composite electrolytes before (pristine) and after (cycled) cycling; and (c) quantification results of the ${}^6\text{Li}$ amount in LLZO, at the PEO/LLZO interface, in decomposed LLZO in TEGDME, and in LiClO_4 in the PEO/TEGDME complex.

LLZO-PEO (LiClO_4)-5 wt% TEGDME composite electrolyte was prepared and cycled using ${}^6\text{Li}$ metal electrodes. The ${}^6\text{Li}$ NMR spectra of the LLZO-PEO (LiClO_4)-5 wt% TEGDME composite before and after ${}^6\text{Li} \rightarrow {}^7\text{Li}$ replacement are shown in Fig. S4† and Table S3.† The result indicates that Li ions mainly pass through the LLZO phase in the LLZO-PEO (LiClO_4)-5 wt%

TEGDME composite, similar to the case of LLZO-PEO (LiClO_4) without TEGDME. PEO, TEGDME, and the interfaces do not contribute significantly to Li-ion conduction.

This finding offers insights that are not only applicable for this composite system but also have relevance for polymer electrolytes with liquid plasticizers. The illustrated Li-ion pathways clearly pinpoint the functional components for Li-ion conduction within complex composite systems, which is useful for guiding effective materials design and engineering for producing high-performance composite electrolytes.

To test the electrochemical properties and stability of the composite electrolyte, the LLZO-PEO (LiClO_4)-TEGDME film was assembled into a symmetric cell using Li metal as electrodes. Electrochemical impedance spectroscopy (EIS) was employed to determine the electrolyte bulk and Li/electrolyte interface impedance and the results are shown in Fig. S5.† Bulk and interface impedance values obtained from the analysis of the EIS spectra in Fig. S5† are listed in Table S4.† The

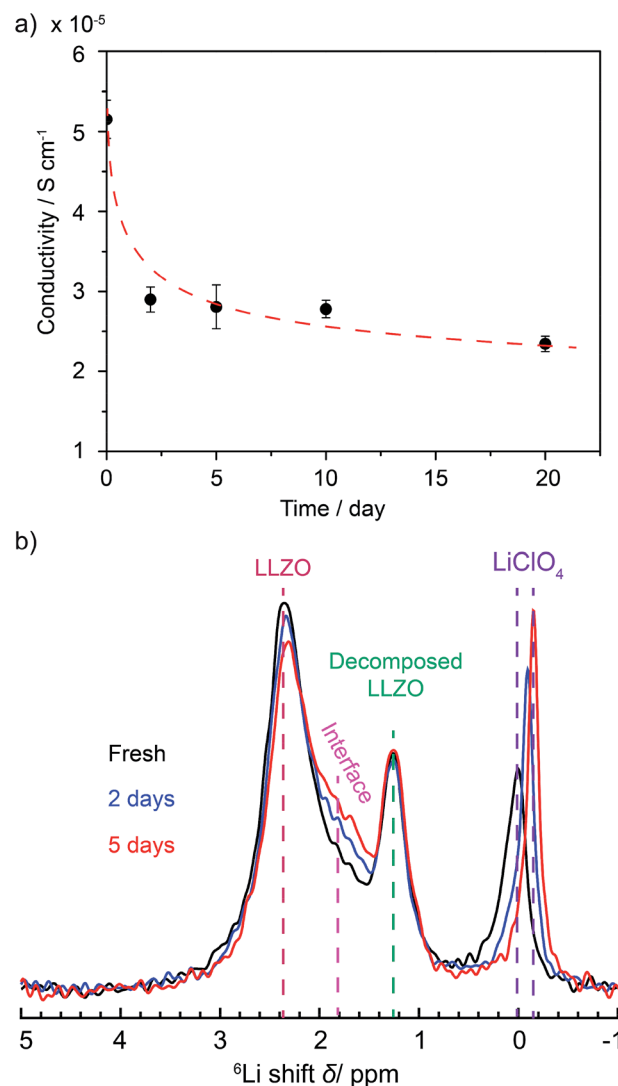


Fig. 4 Stability test of the LLZO-PEO (LiClO_4)-TEGDME composite electrolytes shown as the evolution of (a) conductivity and (b) ${}^6\text{Li}$ NMR spectra with time.

conductivity is calculated using the equation, $\sigma = L/(R_b \times A)$, where L is the thickness of the composite film, R_b is the bulk resistance and A is the contact area between the electrolyte and the electrode. The measured electrolyte bulk conductivities with time are shown in Fig. 4a. Each data point is an average of at least three battery cells with very small deviations to ensure reproducibility. For the freshly made LLZO-PEO (LiClO_4)-TEGDME composite film, the conductivity was $5.15 \times 10^{-5} \text{ S cm}^{-1}$ at room temperature. However, the conductivity decreased with time. A clear drop in conductivity was observed during the first two days, with a decrease to $2.90 \times 10^{-5} \text{ S cm}^{-1}$. Thereafter, the conductivity only showed a slight reduction. After 20 days, the conductivity was $2.34 \times 10^{-5} \text{ S cm}^{-1}$. The ^6Li NMR spectra of the freshly made LLZO-PEO (LiClO_4)-TEGDME sample, and the same sample after it was aged for 2 days and 5 days (Fig. 4b) showed that bulk LLZO resonance at 2.4 ppm decreased slightly over time while the interface species at around 1.8 ppm increased. This suggests that a small fraction of the bulk LLZO is converted into the interface, probably as a result of more TEGDME being absorbed by LLZO over time. In addition, the LiClO_4 resonance gradually shifts to the right, towards higher field, which implies that Li salts dissociate from the PEO/TEGDME complex and dissolve back into pure TEGDME. Since Li conduction is mainly *via* the Li salts within the PEO/TEGDME complex as discussed above, LiClO_4 dissociation from PEO/TEGDME is expected to lower the conductivity. The partition of LiClO_4 in TEGDME and the PEO/TEGDME complex will eventually reach equilibrium, so the decay of conductivity will slow down. As is expected, the decrease of conductivity slows down and levels off gradually.

It is worth mentioning that the Li-ion transference number (T_{Li^+}) of LLZO-PEO (LiClO_4)-TEGDME was determined and a value of 0.35 at room temperature was obtained (Fig. S6 and Table S5†). In previous studies, PEO (LiClO_4) polymer electrolytes exhibited a low T_{Li^+} value of around 0.2.^{32,33} The addition of LLZO and TEGDME to PEO improved T_{Li^+} of the composite electrolytes.

Conclusions

LLZO-PEO (LiClO_4)-TEGDME, as a representative system, embodies ceramic-liquid, polymer-liquid, and ceramic-polymer interfaces, in addition to typical bulk solid electrolytes. This study, using high-resolution Li NMR and an isotope replacement strategy, identifies all Li local environments and their roles in forming Li-ion pathways through the composite electrolyte. In this particular system, Li ions are mainly transported *via* TEGDME-associated phases, not the ceramic LLZO or PEO. This work suggests that ion conduction mechanisms strongly depend on the composition and structure of composite electrolytes.

Conflicts of interest

There are no conflicts to declare.

Acknowledgements

This study is sponsored by the Marion Milligan Mason Award, AAAS, and by the NSF under Grant No. 1508404. All of the solid-state NMR experiments were carried out at the NHMFL supported by the NSF under contract DMR-1157490.

References

- 1 B. Dunn, H. Kamath and J.-M. Tarascon, *Science*, 2011, **334**, 928–935.
- 2 P. Simon and Y. Gogotsi, *Nat. Mater.*, 2008, **7**, 845–854.
- 3 M. Armand and J.-M. Tarascon, *Nature*, 2008, **451**, 652–657.
- 4 J.-M. Tarascon and M. Armand, *Nature*, 2001, **414**, 359–367.
- 5 S. S. Zhang, *J. Power Sources*, 2013, **231**, 153–162.
- 6 S. S. Zhang, *J. Power Sources*, 2007, **164**, 351–364.
- 7 L. Hu and K. Xu, *Proc. Natl. Acad. Sci. U. S. A.*, 2014, **111**, 3205–3206.
- 8 A. Manthiram, X. Yu and S. Wang, *Nat. Rev. Mater.*, 2017, **2**, 16103.
- 9 R. Chen, W. Qu, X. Guo, L. Li and F. Wu, *Mater. Horiz.*, 2016, **3**, 487–516.
- 10 S. Stramare, V. Thangadurai and W. Weppner, *Chem. Mater.*, 2003, **15**, 3974–3990.
- 11 R. Murugan, V. Thangadurai and W. Weppner, *Angew. Chem., Int. Ed.*, 2007, **46**, 7778–7781.
- 12 A. Kuhn, V. Duppel and B. V. Lotsch, *Energy Environ. Sci.*, 2013, **6**, 3548.
- 13 R. L. Sacci, J. M. Black, N. Balke, N. J. Dudney, K. L. More and R. R. Unocic, *Nano Lett.*, 2015, **15**, 2011–2018.
- 14 X. Han, Y. Gong, K. (Kelvin) Fu, X. He, G. T. Hitz, J. Dai, A. Pearse, B. Liu, H. Wang, G. Rubloff, Y. Mo, V. Thangadurai, E. D. Wachsman and L. Hu, *Nat. Mater.*, 2016, **16**, 572–579.
- 15 M. A. Schroeder, A. J. Pearse, A. C. Kozen, X. Chen, K. Gregorczyk, X. Han, A. Cao, L. Hu, S. B. Lee, G. W. Rubloff and M. Noked, *Chem. Mater.*, 2015, **27**, 5305–5313.
- 16 R. C. Agrawal and G. P. Pandey, *J. Phys. D: Appl. Phys.*, 2008, **41**, 223001.
- 17 Z. Xue, D. He and X. Xie, *J. Mater. Chem. A*, 2015, **3**, 19218–19253.
- 18 K. (Kelvin) Fu, Y. Gong, J. Dai, A. Gong, X. Han, Y. Yao, C. Wang, Y. Wang, Y. Chen, C. Yan, Y. Li, E. D. Wachsman and L. Hu, *Proc. Natl. Acad. Sci. U. S. A.*, 2016, **113**, 7094–7099.
- 19 J. Zhang, X. Zang, H. Wen, T. Dong, J. Chai, Y. Li, B. Chen, J. Zhao, S. Dong, J. Ma, L. Yue, Z. Liu, X. Guo, G. Cui and L. Chen, *J. Mater. Chem. A*, 2017, **5**, 4940–4948.
- 20 W. Liu, N. Liu, J. Sun, P.-C. Hsu, Y. Li, H.-W. Lee and Y. Cui, *Nano Lett.*, 2015, **15**, 2740–2745.
- 21 I. Villaluenga, K. H. Wujcik, W. Tong, D. Devaux, D. H. C. Wong, J. M. DeSimone and N. P. Balsara, *Proc. Natl. Acad. Sci. U. S. A.*, 2016, **113**, 52–57.
- 22 Y. Zhao, C. Wu, G. Peng, X. Chen, X. Yao, Y. Bai, F. Wu, S. Chen and X. Xu, *J. Power Sources*, 2016, **301**, 47–53.

- 23 W. Liu, D. Lin, J. Sun, G. Zhou and Y. Cui, *ACS Nano*, 2016, **10**, 11407–11413.
- 24 S. Kalnaus, A. S. Sabau, W. E. Tenhaeff, N. J. Dudney and C. Daniel, *J. Power Sources*, 2012, **201**, 280–287.
- 25 H. Lee, M. Yanilmaz, O. Toprakci, K. Fu and X. Zhang, *Energy Environ. Sci.*, 2014, **7**, 3857–3886.
- 26 S. Chintapalli and R. Frech, *Macromolecules*, 1996, **29**, 3499–3506.
- 27 W. H. Meyer, *Adv. Mater.*, 1998, **10**, 439–448.
- 28 D. Zhou, Y.-B. He, R. Liu, M. Liu, H. Du, B. Li, Q. Cai, Q.-H. Yang and F. Kang, *Adv. Energy Mater.*, 2015, **5**, 1500353.
- 29 J. Zheng, M. Tang and Y.-Y. Hu, *Angew. Chem., Int. Ed.*, 2016, **55**, 12538–12542.
- 30 T. Yang, J. Zheng, Q. Cheng, Y.-Y. Hu and C. K. Chan, *ACS Appl. Mater. Interfaces*, 2017, **9**, 21773–21780.
- 31 A. Natarajan, A. M. Stephan, C. H. Chan, N. Kalarikkal and S. Thomas, *J. Appl. Polym. Sci.*, 2017, **134**, 44594.
- 32 H.-Y. Sun, H.-J. Sohn, O. Yamamoto, Y. Takeda and N. Imanishi, *J. Electrochem. Soc.*, 1999, **146**, 1672–1676.
- 33 S. H. Chung, Y. Wang, L. Persi, F. Croce, S. G. Greenbaum, B. Scrosati and E. Plichta, *J. Power Sources*, 2001, **97**, 644–648.